SCIENCE CHINA
Information Sciences

• RESEARCH PAPER •

September 2021, Vol. 64 192304:1–192304:10
https://doi.org/10.1007/s11432-020-2991-1

Optical true time delay pool based hybrid beamformer enabling centralized beamforming control in millimeter-wave C-RAN systems

Huan HUANG[1], Chongfu ZHANG[1,2*], Muchuan YANG[1], Wei ZHENG[1], Jie PENG[1] & Kun QIU[1]

[1]*School of Information and Communication Engineering, Zhongshan Institute, University of Electronic Science and Technology of China, Chengdu* 611731*, China;*
[2]*School of Electronic Information, University of Electronic Science and Technology of China, Zhongshan Institute, Zhongshan* 528402*, China*

Received 19 March 2020/Revised 17 May 2020/Accepted 20 July 2020/Published online 18 August 2021

Abstract Effectively supporting millimeter-wave (mmWave) beamforming is still a major challenge in 5G cloud radio access network (5G C-RAN) systems with evolved common public radio interface-based (eCPRI-based) fronthaul. Herein, an optical true time delay pool based hybrid beamforming (OTTDP-HBF) scheme, enabling centralized beamforming control, is proposed for mmWave 5G C-RAN systems. The weight control of the OTTDP-HBF is physically implemented by a pre-designed optical wavelength matrix which is mapped from a series of optical carriers. After introducing optical true time delay, this optical wavelength matrix then maps to the defined OTTDP. In this scheme, all physical implementation and the computational processing of analog beamforming can be centrally deployed into a centralized unit or distributed unit (CU/DU). Each active antenna unit (AAU) therefore becomes very simple. For single-user and multi-user scenarios, the OTTDP-based hybrid precoders are formulated respectively. In the developed OTTDP-based multi-user hybrid precoder, the spectral efficiency is improved by making use of all RF chains. For a 9-element uniform planar array deployed at an AAU, a designed example of the OTTDP-HBF is presented, where spectral efficiency curves obtained via different precoding schemes for single-user and multi-user scenarios are compared and discussed respectively.

Keywords optical true time delay, MIMO system, millimeter wave, cloud radio access network, multi-user hybrid precoding

Citation Huang H, Zhang C F, Yang M C, et al. Optical true time delay pool based hybrid beamformer enabling centralized beamforming control in millimeter-wave C-RAN systems. Sci China Inf Sci, 2021, 64(9): 192304, https://doi.org/10.1007/s11432-020-2991-1

1 Introduction

Emerging bandwidth-demanding services in wireless communications, such as virtual/augmented reality and 4K/8K high-definition video, require significant bandwidth [1]. The integration of multiple-input multiple-output (MIMO) and millimeter-wave (mmWave) communications provides a promising approach to meet the traffic requirement [2], where the gain generated from beamforming can compensate for huge path losses in mmWave frequencies [3]. In 5G hot-spot scenarios, plentiful mmWave access points (mmWave-APs) are densely deployed, where each mmWave-AP is usually equipped with several antennas [4]. For example, multiple-antenna technology has been introduced into the 5G split-physical layer (split-PHY) fronthaul architecture, where each mmWave-AP is equipped with 4-element phased-array antennas (PAAs) [5]. Different from massive MIMO systems, a mmWave-AP in highly-dense environments has a small coverage area and only requires a few antennas. To implement these dense mmWave-APs effectively, radio access network (RAN) centralization, i.e., the cloud radio access network (C-RAN), becomes the most widely considered solution [6]. Moreover, the 5G RAN is required to support multiple functional

* Corresponding author (email: cfzhang@uestc.edu.cn)

splits, where a base station is split into a centralized unit (CU), a distributed unit (DU), and an active antenna unit (AAU).

The path and penetration losses are excessive at mmWave frequencies, especially at 60 GHz, thus the beamforming gain generated from PAAs is essential to implement a mmWave system [7, 8]. However, supporting mmWave beamforming effectively is still a major challenge in a 5G C-RAN system with evolved common public radio interface-based (eCPRI-based) fronthaul [9]. In mmWave communications, two widely used hybrid precoding methods are the orthogonal matching pursuit (OMP) based hybrid precoding [10] and the hierarchical hybrid precoding [11]. Based on the hierarchical idea in [11], a digital precoder can be computed by the water-filling solution after determining the analog precoder. Moreover, an important solution for the analog beamforming in the hybrid beamforming is the codebook-based strategy [12–15]. For example, it was assumed that predefined quantization codebooks were employed for analog precoding, and the equally spaced beamsteering vectors constituted the codebooks [14, 15]. In practice, two widely-used codebooks for beamforming are the n-bit beam codebook and the discrete Fourier transform (DFT)-based beam codebook [16, 17].

Moreover, the traditional physical implementation of a beam codebook is based on the weight control of PAAs. Compared with beamforming via electrical phase shifters, beamforming based on optical true time delay (OTTD) has advantages such as low loss, large bandwidth, and none "beam squint" [18, 19]. For example, optical beamforming for a 5G C-RAN system with analog fronthaul links has been presented, where the weight control of optical beamformers was deployed at mmWave-APs [5]. For both optical and electrical beamforming [5, 20], the weight control modules of analog beamforming are mostly deployed at the front end of C-RAN systems, i.e., the APs. Specifically, in a functional-decomposition 5G C-RAN system, analog beamformers are implemented in AAUs, and the control algorithm for beamforming is assumed to reside in the CU/DU. Therefore, deploying weight control modules at dense AAUs inevitably leads to high operating expenditure and capital expenditure. To solve this problem, a centralized beamforming control system has been proposed [21, 22], where these studies are analog beamforming methods. However, the optical beamforming usually belongs to analog beamforming, thus it can only make transmitter power focus on the desired direction [23, 24]. Although we have given a hybrid precoder based on OTTD, this hybrid precoder was only suitable for a single user [25].

In this work, we present an optical true time delay pool based hybrid beamforming (OTTDP-HBF) scheme for mmWave 5G C-RAN systems with eCPRI-based fronthaul, where weight control modules of analog beamforming for all AAUs can be decoupled from PAAs and centralized into the CU/DU. In this scheme, the weight control of analog beamforming is physically implemented by a pre-designed optical wavelength matrix, and the optical wavelength matrix is mapped from a series of optical carriers generated in the CU/DU. After introducing OTTD, the optical wavelength matrix then maps to the defined optical true time delay pool (OTTDP). Instead of employing a series of tunable optical filters (TOFs), only a passive demultiplexer (Demuxer) is employed in each AAU. Therefore, the deployment of plentiful mmWave AAUs is low-cost and low-complexity. A framework of the proposed OTTDP-HBF for a 5G C-RAN system is presented. Taking an AAU as an example, the principles of the proposed OTTDP-HBF scheme is explained, and the physical implementation of the proposed OTTDP-HBF is also introduced. An OTTDP-based hybrid precoding method for the single-user channel is shown to verify the feasibility of the OTTDP-HBF scheme. Moreover, we develop an OTTDP-based multi-user hybrid precoder. The developed multi-user hybrid precoder can make use of RF chains when the number of RF chains is bigger than the total number of users. Therefore, the averaged achievable rate per user is improved when compared with that obtained by the widely-used two-stage multi-user hybrid precoder [13], where we only work the remaining RF chain and add no transmitted power.

We employ capital bold type for a matrix e.g., $\boldsymbol{W}_{\mathrm{OW}}$, small bold type for a vector e.g., $\boldsymbol{p}_s$, and italic type for a scalar e.g., M_t. The superscripts H, T, and -1 respectively represent the Hermitian transpose, transpose, and the inverse of a matrix. The symbol $\|\cdot\|_{\mathrm{F}}$ and $\mathrm{E}[\cdot]$ denote the Fourier norm and the expectation.

2 System mode

Figure 1(a) schematically shows the proposed OTTDP-HBF for mmWave 5G C-RAN systems with eCPRI-based fronthaul, where AAUs, i.e., mmWave-APs are densely deployed, and each mmWave-AP is equipped with a few antennas. In the proposed scheme, a pre-designed optical wavelength matrix is

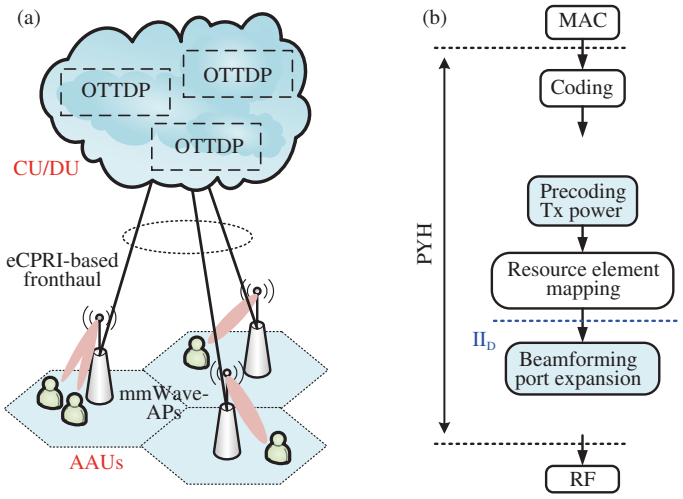

Figure 1 (Color online) (a) Structure of the proposed OTTDP-HBF for mmWave 5G C-RAN systems with eCPRI-based fronthaul; (b) PHY-layer with brief processing stages in downlink direction, and a promising eCPRI split Π_D. OTTDP-HBF: optical true time delay based hybrid beamforming.

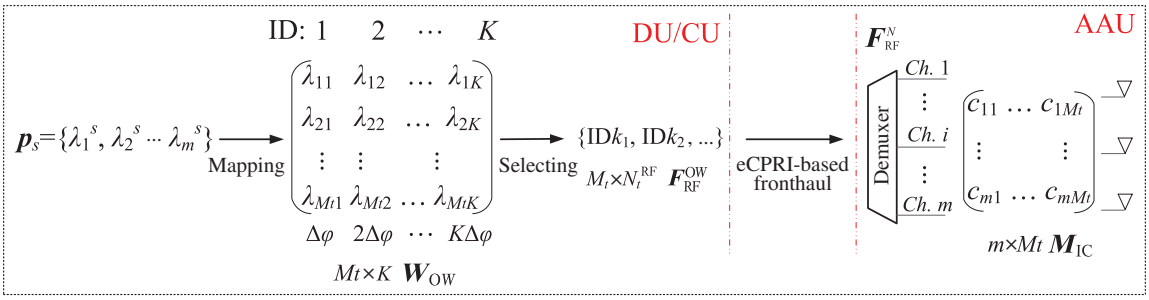

Figure 2 (Color online) Framework of the proposed OTTDP-HBF enabling centralized beamforming control in a mmWave 5G C-RAN system with eCPRI-based fronthaul.

mapped from a series of uniform-spacing optical carriers generated in the CU/DU. After introducing OTTD by a dispersive medium, the pre-designed optical wavelength matrix then maps to the OTTDP.

Specifically, a reference eCPRI split (Split II_D) inside the PHY layer is described in Figure 1(b). Introducing mmWave beamforming into a functional-decomposition 5G C-RAN system, the control algorithm for beamforming is assumed to reside in the CU/DU, but beamformers are implemented in AAUs. Therefore, this control data must be transmitted from the CU/DU to AAUs, which wastes a lot of fronthaul bandwidth. However, in the proposed OTTDP-HBF scheme, the implementation of analog beamforming can be physically deployed at the CU/DU, and the control of analog precoding for all AAUs can also be centralized into the CU/DU. Each mmWave AAU with beamforming via the OTTDP-HBF is simple, so the deployment of dense AAUs becomes easy and cost-advantage.

2.1 Framework of optical true time delay pool based hybrid beamforming

Taking the implementation for an AAU as an example, a framework for the computational modeling and analysis of the proposed OTTDP-HBF enabling centralized beamforming control in the functional-decomposition 5G C-RAN is presented in Figure 2. It is assumed that the fully-connected hybrid beamforming transmitter sends N_s ($N_s \leqslant N_t^{\mathrm{RF}} \leqslant M_t$) data streams and is equipped with M_t antennas and N_t^{RF} RF chains. Firstly, in the CU/DU, m optical carriers with wavelength spacing $\Delta\lambda$ are generated by a multi-wavelength laser source [26], whose optical wavelengths are termed as a $1 \times m$ vector $\boldsymbol{p}_s$.

Secondly, an $M_t \times K$ optical wavelength matrix $\boldsymbol{W}_{\mathrm{OW}}$ is mapped from $\boldsymbol{p}_s$, as shown in Figure 2. The r-th column in $\boldsymbol{W}_{\mathrm{OW}}$ represents M_t optical carriers selected from $\boldsymbol{p}_s$, and these optical carriers can be employed to introduce OTTD and then form a specific beam pattern IDr at the AAU. To support different beam IDs at the same time, a constraint is required to be considered in the mapping process. The constraint is that different elements of $\boldsymbol{W}_{\mathrm{OW}}$ cannot be equal. Moreover, for an $M_t \times K$ $\boldsymbol{W}_{\mathrm{OW}}$, the

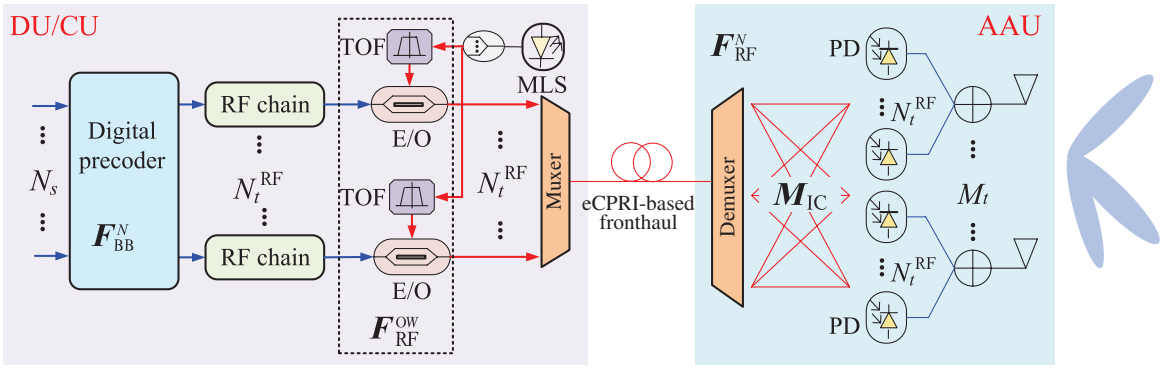

Figure 3 (Color online) Implementation of the proposed OTTDP-HBF in a mmWave 5G C-RAN system with eCPRI-based fronthaul. TOF: tunable optical filter; E/O: electro-optic conversion; MLS: multi-wavelength laser source; Muxer: multiplexer; Demuxer: demultiplexer; PD: photodetector.

number of required optical carriers, i.e., the length of $\boldsymbol{p}_s$ is desired to be as small as possible. Specifically, assume that adjacent elements in the r-th column of the $\boldsymbol{W}_{\mathrm{OW}}$ have a fixed wavelength spacing of $r\Delta\lambda$, the mapping rules of the $\boldsymbol{W}_{\mathrm{OW}}$ can be expressed by

$$\begin{aligned}&\min_{m}\ \boldsymbol{p}_s,\\&\text{s.t. } \lambda_{tr},\lambda_{uv},\lambda_{th}\in\boldsymbol{W}_{\mathrm{OW}},\\&\quad\text{(i) } \lambda_{tr}\neq\lambda_{uv},\ \forall t\neq u\,\&\,r\neq v,\\&\quad\text{(ii) } \lambda_{th}=\lambda_{t1}+t(h-1)\Delta\lambda,\ \forall 1\leqslant h\leqslant M_t.\end{aligned}\tag{1}$$

Because only one RF chain works in analog beamforming at the same time, the OTTDP in [21] is only required to support a beam ID. Hybrid beamforming can provide better performance than that of analog beamforming, where N_t^{RF} RF chains work simultaneously. Therefore, the constraint (i) expressed in (1) is stronger compared with that in [21, 22], and this enables the $\boldsymbol{W}_{\mathrm{OW}}$ to support N_t^{RF} beam IDs simultaneously.

Thirdly, N_t^{RF} columns are selected from the determined $\boldsymbol{W}_{\mathrm{OW}}$ and employed to form an $M_t\times N_t^{\mathrm{RF}}$ matrix $\boldsymbol{F}_{\mathrm{RF}}^{\mathrm{OW}}$. The optical carriers corresponding to the $\boldsymbol{F}_{\mathrm{RF}}^{\mathrm{OW}}$ are selected from $\boldsymbol{p}_s$ and then employed to carry out RF chains to the AAU.

Finally, the desired OTTD can be introduced into each RF chain by a dispersive medium like a single-mode fiber (SMF). Namely, the matrix $\boldsymbol{F}_{\mathrm{RF}}^{\mathrm{OW}}$ transforms into the analog precoding matrix $\boldsymbol{F}_{\mathrm{RF}}^{N}$ after introducing OTTD, as illustrated in Figure 2. Besides, the optical wavelength matrix $\boldsymbol{W}_{\mathrm{OW}}$ is corresponding to a fixed OTTDP after introducing OTTD. For the implementation of different analog precoding, different N_t^{RF} columns of $\boldsymbol{W}_{\mathrm{OW}}$ are selected.

Instead of deploying a series of TOFs [27], a passive Demuxer is employed in the AAU to minimize its cost and complexity, as displayed in Figure 2. Moreover, m channels of the Demuxer must match elements in the $\boldsymbol{p}_s$, thus an $m\times M_t$ matrix $\boldsymbol{M}_{\mathrm{IC}}$ is defined to describe the interconnection between the channels and antennas. The element c_{ir} in the $\boldsymbol{M}_{\mathrm{IC}}$ is "1" or "0", which represents the i-th channel and the r-th antenna is connected or not. More details about this interconnection matrix can refer to [21].

2.2 Implementation of optical true time delay pool based hybrid beamforming

The physical implementation of the proposed OTTDP-HBF can be seen in Figure 3. Firstly, the power of N_s data streams is adjusted according to the $\boldsymbol{F}_{\mathrm{BB}}^{N}$. The analog beamformer performs specific phase-shift values for RF chains, and the phase-shift values between antennas in the proposed OTTD-HBF scheme are introduced by an SMF. The relationship between the phase-shift difference and elements in the $\boldsymbol{W}_{\mathrm{OW}}$ is

$$(t-i)k\Delta\varphi=(\lambda_{tk}-\lambda_{ik})(2\pi c/\lambda_{\mathrm{RF}})DL,\tag{2}$$

where D and L represent the dispersion coefficient and the length of SMF, λ_{RF} is the wavelength of each RF chain, and the phase-shift unit $\Delta\varphi$ satisfies the equation that is $K\Delta\varphi=2\pi$.

Secondly, the uniformly-spaced optical carriers generated from the MLS are split into N_t^{RF} branches, and each branch is used for providing M_t optical carriers corresponding to a column of the $\boldsymbol{F}_{\mathrm{RF}}^{\mathrm{OW}}$. The TOF

modules are employed to select these specific optical carriers, and N_t^{RF} RF chains are then modulated on these selected optical carriers.

Thirdly, a multiplexer (Muxer) is introduced and then those modulated optical carriers are injected into the eCPRI-based fronthaul link. Each optical carrier has a specific wavelength, so the required OTTD values are introduced into RF chains. Because optical carriers match channels of the Demuxer deployed in the AAU, the optical carriers can be separated by the Demuxer. Finally, the modulated optical carriers are detected by photodetectors (PDs), and different phase-shift values are then introduced into antennas.

Similarly, all AAUs can be deployed based on the proposed OTTDP-HBF scheme, where each AAU only requires a passive Demuxer instead of expensive TOFs. Moreover, the beamforming control functions for all AAUs and the physical implementation of analog beamforming can be centralized into the CU/DU, which is adapted to the characteristic of the 5G C-RAN system with eCPRI-based fronthaul.

3 OTTDP-based hybrid precoding for mmWave communications

Compared with the work about OTTDP-based analog beamforming in [21], precoding processes are required for the proposed OTTDP-HBF. In mmWave communications, the wireless channel $\boldsymbol{H}$ can be expressed based on the clustered channel model [10, 11],

$$\boldsymbol{H} = \left(\sqrt{M_t M_r / N_c N_l}\right) \sum_{c=1}^{N_c} \sum_{l=1}^{N_l} \beta_{cl} \boldsymbol{a}_R(\phi_{cl}, \varphi_{cl}) \boldsymbol{a}_T^{\mathrm{H}}(\theta_{cl}, \vartheta_{cl}), \tag{3}$$

where N_c denotes the number of scattering clusters, and each cluster has N_l propagation paths, β_{cl} is the complex gain of the l-th path in the c-th cluster, ϕ_{cl} (φ_{cl}) and θ_{cl} (ϑ_{cl}) represent the arrival and the departure azimuth (elevation) angles, and $\boldsymbol{a}_R$ and $\boldsymbol{a}_T$ are the normalized receive and the normalized transmit array responses. In practice, the mmWave wireless channel matrix can be obtained by channel state information (CSI) [28] or channel estimation [15, 29].

3.1 OTTDP-based sparse precoding for the single-user mmWave channel

Consider a single-user scenario, and we assume that the user is equipped with M_r antennas and N_r^{RF} RF chains. The mmWave wireless channel mode $\boldsymbol{H}$ expressed in (3) satisfies a constant that $\mathrm{E}[\|\boldsymbol{H}\|_{\mathrm{F}}^2] = M_t M_r$. If a Gaussian signal is transmitted and the average signal received power is ρ, the overall spectral efficiency R can be expressed as [10]

$$R = \log_2 \left(\left| \boldsymbol{I}_{Ns} + \frac{\rho}{N_s \sigma^2} \boldsymbol{K}^{-1} \boldsymbol{W}_{\mathrm{BB}}^{\mathrm{H}} \boldsymbol{W}_{\mathrm{RF}}^{\mathrm{H}} \boldsymbol{H} \boldsymbol{F}_{\mathrm{RF}} \boldsymbol{F}_{\mathrm{BB}} \boldsymbol{F}_{\mathrm{BB}}^{\mathrm{H}} \boldsymbol{F}_{\mathrm{RF}}^{\mathrm{H}} \boldsymbol{H}^{\mathrm{H}} \boldsymbol{W}_{\mathrm{RF}} \boldsymbol{W}_{\mathrm{BB}} \right| \right), \tag{4}$$

where σ^2 is the variance of the i.d.d. noise $\boldsymbol{n}$, and $\boldsymbol{n} \sim \mathcal{CN}(0, \sigma^2 \boldsymbol{I}_{M_r})$, $\boldsymbol{K} = \boldsymbol{W}_{\mathrm{BB}}^{\mathrm{H}} \boldsymbol{W}_{\mathrm{RF}}^{\mathrm{H}} \boldsymbol{W}_{\mathrm{RF}} \boldsymbol{W}_{\mathrm{BB}}$, $\boldsymbol{W}_{\mathrm{RF}}$ and $\boldsymbol{W}_{\mathrm{BB}}$ represent the analog and the digital combining matrices at a receiver, $\boldsymbol{F}_{\mathrm{RF}}$ and $\boldsymbol{F}_{\mathrm{BB}}$ represent the analog and the digital precoding matrices at a transmitter, and $\boldsymbol{I}_{Ns}$ is the unit matrix.

The solution of the spectral efficiency maximization (SEM) problem expressed by (4) can be approximately translated into finding the feasible analog and digital precoding matrices $\boldsymbol{F}_{\mathrm{RF}}^N$ and $\boldsymbol{F}_{\mathrm{BB}}^N$, where $\|\boldsymbol{F}_{\mathrm{RF}}^N \boldsymbol{F}_{\mathrm{BB}}^N\|_{\mathrm{F}}^2 = N_s$. The $\boldsymbol{F}_{\mathrm{RF}}^N$ is physically implemented by the $\boldsymbol{F}_{\mathrm{RF}}^{\mathrm{OW}}$ in the proposed OTTDP-HBF scheme. After determining the analog precoding matrices $\boldsymbol{F}_{\mathrm{RF}}^N$, the corresponding columns are selected from the $\boldsymbol{W}_{\mathrm{OW}}$ to form the $\boldsymbol{F}_{\mathrm{RF}}^{\mathrm{OW}}$. After introducing OTTD, the $\boldsymbol{F}_{\mathrm{RF}}^{\mathrm{OW}}$ then maps to the analog precoding matrix $\boldsymbol{F}_{\mathrm{RF}}^N$.

Next, the hybrid precoding method for the proposed OTTDP-based HBF is presented. According to (2), a shift-phase difference matrix can be generated based on the $\boldsymbol{F}_{\mathrm{RF}}^{\mathrm{OW}}$, where the shift-phase difference is introduced by OTTD. After introducing OTTD, the optical wavelength matrix $\boldsymbol{W}_{\mathrm{OW}}$ then maps to the defined OTTDP that is employed to implement analog precoding in the proposed OTTDP-HBF scheme. Therefore, according to the $\boldsymbol{W}_{\mathrm{OW}}$, a weight matrix $\boldsymbol{F}_w^{\mathrm{OW}}$ that is similar to a DFT-based codebook is then defined as

$$\begin{aligned} \boldsymbol{F}_w^{\mathrm{OW}} &= \left\{ w_{tr} \middle| w_{tr} = \frac{1}{\sqrt{M_t}} \mathrm{e}^{\mathrm{j}(t-1)r\Delta\varphi},\ 1 \leqslant t \leqslant M_t,\ 1 \leqslant r \leqslant K \right\}, \\ &= [\boldsymbol{w}_1, \boldsymbol{w}_2, \ldots, \boldsymbol{w}_K], \end{aligned} \tag{5}$$

where $j^2 = -1$, and $\boldsymbol{w}_p$ is the p-th codeword under the normalization constraint $\|\boldsymbol{w}_p\|_{\mathrm{F}}^2 = 1$. The number of beam IDs K in the $\boldsymbol{F}_w^{\mathrm{OW}}$ is arbitrary when compared with that in the DFT-based codebook [17, 30]. Namely, the number of beam IDs is not required to be an integer multiple of the number of antennas M_t.

A widely used hybrid precoding algorithm for the single-user mmWave channel is the OMP-based sparse precoding algorithm, where the difference between the optimal fully-digital precoding matrix $\boldsymbol{F}_{\mathrm{opt}}$ and the overall matrix $\boldsymbol{F}_{\mathrm{RF}}^{\mathrm{OMP}}\boldsymbol{F}_{\mathrm{BB}}^{\mathrm{OMP}}$ possesses the minimum Frobenius norm [10]. For a single-user hybrid beamforming system, an analog precoder can be chosen from a pre-designed codebook. Therefore, based on the OMP-based sparse precoding algorithm and the weight matrix $\boldsymbol{F}_w^{\mathrm{OW}}$ in (5), the hybrid precoding method for the proposed OTTDP-HBF scheme is summarized as Algorithm 1.

Algorithm 1 OTTDP-based sparse precoding via orthogonal matching pursuit

Input: $\boldsymbol{F}_{\mathrm{opt}}$, $\boldsymbol{W}_{\mathrm{OW}}$, and $\boldsymbol{F}_w^{\mathrm{OW}}$.
Output: $\boldsymbol{F}_{\mathrm{RF}}^{\mathrm{OW}}$ and $\boldsymbol{F}_{\mathrm{BB}}^{N}$.
1: Initialize $\boldsymbol{F}_{\mathrm{RF}}^{N}$ and $\boldsymbol{F}_{\mathrm{BB}}^{N}$;
2: $\boldsymbol{R}_{\mathrm{res}} = \boldsymbol{F}_{\mathrm{opt}}$;
3: **for** $i = 1 \to N_t^{\mathrm{RF}}$ **do**
4: $\quad k = \arg\max_{p\in[1,\ldots,K],\boldsymbol{w}_p\subset\boldsymbol{F}_w^{\mathrm{OW}}} |\langle \boldsymbol{w}_p, \boldsymbol{R}_{\mathrm{res}}\rangle|$;
5: $\quad \boldsymbol{F}_{\mathrm{RF}}^{N} = \boldsymbol{F}_{\mathrm{RF}}^{N} \cup \boldsymbol{w}_k$;
6: $\quad \boldsymbol{F}_{\mathrm{BB}}^{N} = [(\boldsymbol{F}_{\mathrm{RF}}^{N})^{\mathrm{H}}\boldsymbol{F}_{\mathrm{RF}}^{N}]^{-1}(\boldsymbol{F}_{\mathrm{RF}}^{N})^{\mathrm{H}}\boldsymbol{F}_{\mathrm{opt}}$;
7: $\quad \boldsymbol{R}_{\mathrm{res}} = \frac{\boldsymbol{F}_{\mathrm{opt}}-\boldsymbol{F}_{\mathrm{RF}}^{N}\boldsymbol{F}_{\mathrm{BB}}^{N}}{\|\boldsymbol{F}_{\mathrm{opt}}-\boldsymbol{F}_{\mathrm{RF}}^{N}\boldsymbol{F}_{\mathrm{BB}}^{N}\|_{\mathrm{F}}}$;
8: **end for**
9: Select $\boldsymbol{F}_{\mathrm{RF}}^{\mathrm{OW}}$ from $\boldsymbol{W}_{\mathrm{OW}}$ according to $\boldsymbol{F}_{\mathrm{RF}}^{N}$.

3.2 OTTDP-based sparse precoding for the multi-user mmWave channel

Consider a multi-user scenario, where the number of users is N_u. We assume that the total number of data streams N_s is equal to N_u. Namely, one mmWave-AP equipped with M_t antennas and N_t^{RF} RF chains communicates with every user via one data stream. The codebook-based hybrid precoding methods can be also employed for multi-user scenarios [12, 13, 31]. By meeting a performance metric such as the system sum-rate, some codewords, i.e., some beamsteering vectors are selected from a beam codebook to form the analog precoder. Generally, the multi-user codebook-based hybrid precoding suffers from a limitation that the number of working RF chains is equal to the total number of users. Therefore, this method cannot make full use of all N_t^{RF} RF chains when the total number of RF chains is larger than the number of users.

The wireless channel $\boldsymbol{H}_i$ between the i-th user and the mmWave-AP can be molded by (3), and the achievable rate of the i-th user is then [13],

$$R_i = \log_2\left(1 + \frac{\frac{P}{N_u}|\boldsymbol{H}_i\boldsymbol{F}_{\mathrm{RF}}\boldsymbol{F}_i^{\mathrm{BB}}|^2}{\frac{P}{N_u}\sum_{n\neq i}|\boldsymbol{H}_i\boldsymbol{F}_{\mathrm{RF}}\boldsymbol{F}_n^{\mathrm{BB}}|^2 + \sigma^2}\right), \tag{6}$$

where P is the average total transmitted power, and we assume that the transmitter applies the analog precoder $\boldsymbol{F}_{\mathrm{RF}} = [\boldsymbol{F}_1^{\mathrm{RF}}, \boldsymbol{F}_2^{\mathrm{RF}}, \ldots, \boldsymbol{F}_{N_t^{\mathrm{RF}}}^{\mathrm{RF}}]$ and the digital precoder $\boldsymbol{F}_{\mathrm{BB}} = [\boldsymbol{F}_1^{\mathrm{BB}}, \boldsymbol{F}_2^{\mathrm{BB}}, \ldots, \boldsymbol{F}_{N_s}^{\mathrm{BB}}]$. The system sum-rate is then $R_{\mathrm{total}} = \sum_{i=1}^{N_u} R_i$. The hybrid precoding in the transmitter aims to find an available analog and digital precoder. Different from the solution of the SEM problem, multi-user interference must be considered in the precoding for the total spectral efficiency maximization (TSEM) problem.

As stated above, an alternative solution of the TSEM problem is to select an optimal beamsteering vector from a beam codebook for a user. However, it is difficult to make full use of all RF chains when the total number of RF chains is larger than the number of users. Here, we develop a precoding method for multi-user scenarios in the proposed OTTDP-HBF system, which can make full use of all RF chains ($N_t^{\mathrm{RF}} \geqslant N_u$) and can be seen from Algorithm 2. In the proposed OTTDP-HBF scheme, the physical implementation of an analog precoder is based on OTTDP, thus the analog precoder in the proposed scheme is equivalent to selecting suitable columns from $\boldsymbol{W}_{\mathrm{OW}}$.

Firstly, the fully-digital zero-forcing precoder $\boldsymbol{V}_{\mathrm{opt}}$ that is an $M_t \times N_u$ matrix can be computed by [32],

$$\boldsymbol{V}_{\mathrm{opt}} = \boldsymbol{H}^{\mathrm{H}}(\boldsymbol{H}\boldsymbol{H}^{\mathrm{H}})^{-1} = [\boldsymbol{v}_1, \boldsymbol{v}_2, \ldots, \boldsymbol{v}_{N_u}], \tag{7}$$

where $\boldsymbol{H} = [\boldsymbol{H}_1^{\mathrm{T}}, \boldsymbol{H}_2^{\mathrm{T}}, \ldots, \boldsymbol{H}_{N_u}^{\mathrm{T}}]^{\mathrm{T}}$ is the multi-user channel.

Algorithm 2 OTTDP-based hybrid precoding for multi-user scenarios

Input: $\boldsymbol{V}_{\rm opt}$, $\boldsymbol{F}_w^{\rm OW}$, and $\boldsymbol{W}_{\rm OW}$.
Output: $\boldsymbol{V}_{\rm RF}^{\rm OW}$, $\boldsymbol{V}_{\rm RF}$, and $\boldsymbol{V}_{\rm BB}$.
1: Calculate fully-digital zero-forcing precoder $\boldsymbol{V}_{\rm opt}$ by (7);
2: Calculate weight vector $\boldsymbol{h}$ by (9);
3: Generate analog precoder $\boldsymbol{V}_{\rm RF}$ by (10);
4: Select columns from $\boldsymbol{W}_{\rm OW}$ to form $\boldsymbol{V}_{\rm RF}^{\rm OW}$;
5: Calculate digital precoder $\boldsymbol{V}_{\rm BB}$ by (11).

Secondly, a pre-designed OTTDP-based weight matrix $\boldsymbol{F}_w^{\rm OW}$ is obtained by (5), and then every column of $\boldsymbol{V}_{\rm opt}$ in (7) is decomposed on columns of $\boldsymbol{F}_w^{\rm OW}$,

$$\boldsymbol{v}_i \Leftrightarrow [x_{1i}\boldsymbol{w}_1, x_{2i}\boldsymbol{w}_2, \ldots, x_{Ki}\boldsymbol{w}_K], \tag{8}$$

where $x_{ti} = \langle \boldsymbol{w}_t, \boldsymbol{v}_i \rangle$ is the inner product of $\boldsymbol{w}_t$ and $\boldsymbol{v}_i$, and $\boldsymbol{v}_i \subset \boldsymbol{V}_{\rm opt}$. A weight vector $\boldsymbol{h}$ with K elements is then defined as

$$\boldsymbol{h} = \left\{ h_t \middle| h_t = \sum_{i=1}^{N_u} x_{ti}, 1 \leqslant t \leqslant K \right\}. \tag{9}$$

Thirdly, find the largest $N_t^{\rm RF}$ elements from $\boldsymbol{h}$ that is termed as $\{h_{e1}, h_{e2}, \ldots, h_{e_{N_t^{\rm RF}}}\}$. According to the subscripts $\{e_1, e_2, \ldots, e_{N_t^{\rm RF}}\}$, the corresponding codewords are then selected from $\boldsymbol{F}_w^{\rm OW}$, which form the analog precoder $\boldsymbol{V}_{\rm RF}$ in the proposed OTTDP-based multi-user hybrid precoder,

$$\boldsymbol{V}_{\rm RF} = \left[\boldsymbol{w}_{e1}, \boldsymbol{w}_{e2}, \ldots, \boldsymbol{w}_{e_{N_t^{\rm RF}}} \right]. \tag{10}$$

The physical implementation of the analog precoder is based on OTTDP. Therefore, the corresponding columns are selected from $\boldsymbol{W}_{\rm OW}$ according to the calculated $\boldsymbol{V}_{\rm RF}$, and then form the matrix $\boldsymbol{V}_{\rm RF}^{\rm OW}$.

Finally, based on (9), an equivalent channel between the i-th user and the transmitter can be defined as $\boldsymbol{H}_i^e = \boldsymbol{H}_i \boldsymbol{V}_{\rm RF}$. Therefore, the equivalent multi-user channel can be written as $\boldsymbol{H}^e = [(\boldsymbol{H}_1^e)^{\rm T}, (\boldsymbol{H}_2^e)^{\rm T}, \ldots, (\boldsymbol{H}_{N_u}^e)^{\rm T}]^{\rm T}$. According to the equivalent multi-user channel and the zero-forcing precoding, the multi-user interference can be completely suppressed by the digital precoder $\boldsymbol{V}_{\rm BB}$ that has the following form:

$$\boldsymbol{V}_{\rm BB} = (\boldsymbol{H}^e)^{\rm H}[\boldsymbol{H}^e(\boldsymbol{H}^e)^{\rm H}]^{-1}\boldsymbol{P}^{\frac{1}{2}} = \boldsymbol{V}_{\rm ZF}\boldsymbol{P}^{\frac{1}{2}}, \tag{11}$$

where $\boldsymbol{P} = {\rm diag}(p_1, \ldots, p_{N_u})$ with p_i ($\sum_{i=1}^{N_u} p_i = P$) denoting the transmit power allocated to the i-th user can be determined via the well-known water-pouring algorithm.

4 Designed example and result discussion

Consider a 9-element uniform planar array (UPA) deployed at a mmWave AAU in a 5G C-RAN system, i.e., $M_t = 9$. Setting K=10, the designed example of a 9×10 $\boldsymbol{W}_{\rm OW}$ and its corresponding weight matrix $\boldsymbol{F}_w^{\rm OW}$ are shown in Figure 4. This 9×10 optical wavelength matrix $\boldsymbol{W}_{\rm OW}$ can be physically implemented by a 1×165 $\boldsymbol{p}_s$. In the proposed OTTDP-HBF scheme, the physical implementation and the control of analog precoding for different mmWave AAUs are centralized at the CU/DU, where we only employ a passive Demuxer instead of expensive TOFs [27] at every AAU. Therefore, based on the proposed scheme, the deployment of plentiful mmWave AAUs is low-cost and low-complexity.

4.1 Example of OTTDP-based sparse precoding for a single user

We verify the feasibility of the proposed OTTDP-HBF scheme for a single user, where we assume that the number of RF chains is equal to 3, i.e., $N_t^{\rm RF} = 3$, and the number of receiving antennas is 4. For simplicity, it is assumed that the combining matrix at the user is generated by the fully-digital precoding. Based on (3), the single-user mmWave channel $\boldsymbol{H}$ is modeled by setting $N_c = 6$ and $N_l = 1$. In the numerical simulation, it is assumed that N_s is equal to 1, 2, as well as 3. All results in Figure 5 are obtained from 500 Monte-Carlo trials.

In Figure 5, the spectral efficiency curves via the fully-digital precoding (red color) and the OMP-based hybrid precoding [10] (blue color) are given as comparisons, where the received signal-to-noise ratio (SNR)

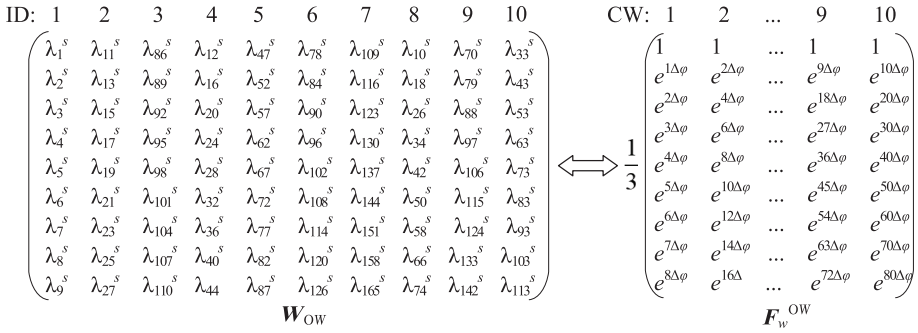

Figure 4 An example of 9×10 optical wavelength matrix $\boldsymbol{W}_{\mathrm{OW}}$ designed based on (1), and its corresponding weight matrix $\boldsymbol{F}_w^{\mathrm{OW}}$. CW: codeword.

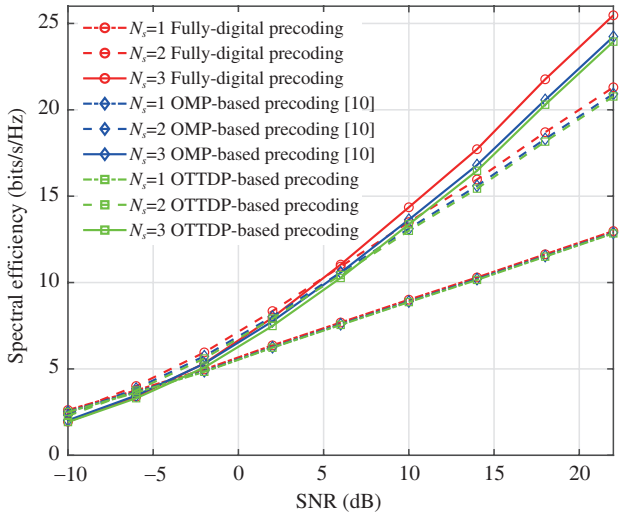

Figure 5 (Color online) Spectral efficiency versus SNR (ρ/σ^2) for the single user channel via fully-digital precoding (red color), OMP-based hybrid precoding (blue color), and OTTDP-based hybrid precoding (green color).

is defined as ρ/σ^2. Moreover, the spectral efficiency curve via the proposed OTTDP-based precoding is depicted in Figure 5 by green color. Compared with the OMP-based precoding , a fixed 9×10 weight matrix $\boldsymbol{F}_w^{\mathrm{OW}}$ is employed in the proposed OTTDP-based hybrid precoding, which is corresponding to the $\boldsymbol{W}_{\mathrm{OW}}$. The analog precoding matrix $\boldsymbol{F}_{\mathrm{RF}}^N$ is computed based on the fixed $\boldsymbol{F}_w^{\mathrm{OW}}$ rather than the time-varying array responses, which leads to a slight degradation in performance. However, the OMP-based hybrid precoding is physically implemented by precise phase shifters. In the proposed scheme, we introduce the fixed $\boldsymbol{F}_w^{\mathrm{OW}}$ that is physically built by a multi-wavelength laser source to implement the OTTDP-HBF.

4.2 Example of OTTDP-based multi-user hybrid precoder

We also consider a multi-user scenario, where a mmWave AAU with a 9-element UPA communicates with two users and each user is assumed to have a single antenna. Moreover, the total number of RF chains is 3. All the rates plotted in Figure 6 are the averaged achievable rates per user which can be written as $\mathrm{E}[\frac{1}{N_u}\sum_{i=1}^{N_u} R_i]$ with R_i in (6), where the transmit SNR is defined as (P/σ^2). The total transmitted power of the precoders shown in Figure 6 is the same. The spectral efficiency curve generated via a fully-digital zero-forcing precoder is given as a comparison and marked by red color. Based on the widely-used two-stage multi-user hybrid precoder [13], the spectral efficiency curve is also obtained and marked by green color, where only two RF chains are working.

According to Algorithm 2, the spectral efficiency curve is also illustrated in Figure 6 by blue color, where the designed 9×10 $\boldsymbol{W}_{\mathrm{OW}}$ is used. Because all RF chains are utilized, the averaged achievable rates are improved when compared with that obtained by the two-stage multi-user hybrid precoder. We only work the remaining RF chain and add no transmitted power. Moreover, the proposed OTTDP-based multi-user precoder can be centrally controlled and deployed.

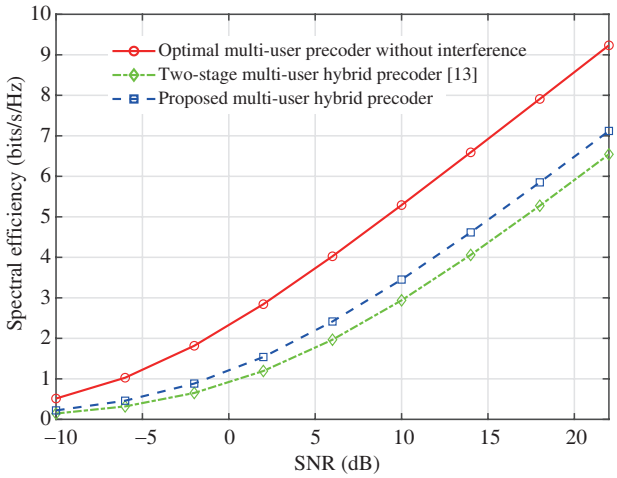

Figure 6 (Color online) Averaged achievable rates achieved by optimal multi-user precoder without interference (red color), two-stage multi-user hybrid precoder (green color), and OTTDP-based multi-user precoder (blue color).

5 Conclusion

In this work, an OTTDP-HBF enabling centralized beamforming control has been proposed for mmWave 5G C-RAN systems with eCPRI-based fronthaul. In this scheme, all physical implementation and the computational processing of analog beamforming were centrally deployed into the CU/DU, and a passive Demuxer was deployed at each AAU instead of a series of TOFs. For single-user and multi-user scenarios, the OTTDP-based hybrid precoding methods were also formulated. For a 9-element UPA, a designed example of the OTTDP-HBF was presented, where the 9×10 optical wavelength matrix $\boldsymbol{W}_{\mathrm{OW}}$ and its corresponding weight matrix after introducing OTTD were given. Based on the OMP algorithm and the OTTDP, we considered a single-user scenario and verified the feasibility of the proposed OTTDP-HBF, where the spectral efficiency curve was compared with that via the fully-digital precoding and the OMP-based hybrid precoding. Moreover, we developed an OTTDP-based multi-user hybrid precoder by making use of all RF chains, and the averaged achievable rate per user was improved when compared with that obtained by the widely-used two-stage multi-user hybrid precoder.

Acknowledgements This work was supported by National Key R&D Program of China (Grant No. 2018YFB1801302) and Project for Zhongshan Social Public Welfare Science (Grant No. 2019B2007).

References

1 Li X Y, Yu J J, Chang G-K. Photonics-assisted technologies for extreme broadband 5G wireless communications. J Lightwave Technol, 2019, 37: 2851–2865
2 Xie T, Dai L L, Ng D W K, et al. On the power leakage problem in millimeter-wave massive MIMO with lens antenna arrays. IEEE Trans Signal Process, 2019, 67: 4730–4744
3 Kutty S, Sen D. Beamforming for millimeter wave communications: an inclusive survey. IEEE Commun Surv Tut, 2016, 18: 949–973
4 Jaber M, Imran M A, Tafazolli R, et al. 5G backhaul challenges and emerging research directions: a survey. IEEE Access, 2016, 4: 1743–1766
5 Kalfas G, Vagionas C, Antonopoulos A, et al. Next generation fiber-wireless fronthaul for 5G mmWave networks. IEEE Commun Mag, 2019, 57: 138–144
6 Li H B, Yang Q, Fu S N, et al. Digital code-division multiplexing channel aggregation for mobile fronthaul architecture with low complexity. IEEE Photonics J, 2018, 10: 1–10
7 Gong S Q, Xing C W, Fei Z S, et al. Cooperative beamforming design for physical-layer security of multi-hop MIMO communications. Sci China Inf Sci, 2016, 59: 062304
8 Liu D L, Wu F, Quan X, et al. Energy- and spectral-efficiency of zero-forcing beamforming in massive MIMO systems with imperfect reciprocity calibration: bound and optimization. Sci China Inf Sci, 2018, 61: 122302
9 Alimi I A, Teixeira A L, Monteiro P P. Toward an efficient C-RAN optical fronthaul for the future networks: a tutorial on technologies, requirements, challenges, and solutions. IEEE Commun Surv Tut, 2018, 20: 708–769
10 Ayach O E, Rajagopal S, Abu-Surra S, et al. Spatially sparse precoding in millimeter wave MIMO systems. IEEE Trans Wirel Commun, 2014, 13: 1499–1513
11 Sohrabi F, Yu W. Hybrid digital and analog beamforming design for large-scale antenna arrays. IEEE J Sel Top Signal Process, 2016, 10: 501–513
12 He S W, Wang J H, Huang Y M, et al. Codebook-based hybrid precoding for millimeter wave multiuser systems. IEEE Trans Signal Process, 2017, 65: 5289–5304
13 Alkhateeb A, Leus G, Heath R W. Limited feedback hybrid precoding for multi-user millimeter wave systems. IEEE Trans Wirel Commun, 2015, 14: 6481–6494

14 Alkhateeb A, Heath R W. Frequency selective hybrid precoding for limited feedback millimeter wave systems. IEEE Trans Commun, 2016, 64: 1801–1818
15 Alkhateeb A, Ayach O E, Leus G, et al. Channel estimation and hybrid precoding for millimeter wave cellular systems. IEEE J Sel Top Signal Process, 2014, 8: 831–846
16 Wang J Y, Lan Z, Pyo C-W, et al. Beam codebook based beamforming protocol for multi-Gbps millimeter-wave WPAN systems. IEEE J Sel Areas Commun, 2009, 27: 1390–1399
17 Adhikary A, Nam J, Ahn J-Y, et al. Joint spatial division and multiplexing-the large-scale array regime. IEEE Trans Inform Theory, 2013, 59: 6441–6463
18 Riza N A. Optical multiple beamforming systems for wireless communication antennas. In: Proceedings of SPIE, San Diego, 1995. 139–150
19 Cao Z Z, Ma Q, Smolders A B, et al. Advanced integration techniques on broadband millimeter-wave beam steering for 5G wireless networks and beyond. IEEE J Quantum Electron, 2016, 52: 1–20
20 Bantavis P I, Kolitsidas C I, Empliouk T, et al. A cost-effective wideband switched beam antenna system for a small cell base station. IEEE Trans Antennas Propagat, 2018, 66: 6851–6861
21 Huang H, Zhang C F, Chen C, et al. Optical true time delay pools based centralized beamforming control for wireless base stations phased-array antennas. J Lightwave Technol, 2018, 36: 3693–3699
22 Wang R F, Zhang C F, Huang H, et al. An algorithm approach to optical true time delay pool enabled centralized control beamforming for wireless base station. In: Proceedings of the 17th International Conference on Optical Communications and Networks (ICOCN 2018), Zhuhai, 2018
23 Riza N A. An acoustooptic-phased-array antenna beamformer for multiple simultaneous beam generation. IEEE Photon Technol Lett, 1992, 4: 807–809
24 Zhang L H, Li M, Shi N N, et al. Photonic true time delay beamforming technique with ultra-fast beam scanning. Opt Express, 2017, 25: 14524–14532
25 Huang H, Zhang C F, Yang M C, et al. Optical codebook based hybrid precoding for millimeter wave MIMO systems with fronthaul. In: Proceedings of Asia Communications and Photonics Conference (ACP 2019), Chengdu, 2019
26 Ryu H Y, Lee D, Park K-D, et al. Discretely tunable erbium-doped fiber ring laser selecting ITU-T grids of 273 channels×50-GHz spacing in C- and L-band regions. Appl Phys B, 2004, 79: 583–586
27 Ye X W, Zhang F Z, Pan S L. Optical true time delay unit for multibeamforming. Opt Express, 2015, 23: 10002–10008
28 Chen S Z, Gao Q B, Chen R H, et al. A CSI acquisition approach for mmWave massive MIMO. China Commun, 2019, 16: 1–14
29 Huang C W, Liu L, Yuan C, et al. Iterative channel estimation using LSE and sparse message passing for mmWave MIMO systems. IEEE Trans Signal Process, 2019, 67: 245–259
30 Hung W L, Chen C H, Liao C C, et al. Low-complexity hybrid precoding algorithm based on orthogonal beamforming codebook. In: Proceedings of IEEE Workshop on Signal Processing Systems (SiPS), Hangzhou, 2019
31 Liang L, Xu W, Dong X D. Low-complexity hybrid precoding in massive multiuser MIMO systems. IEEE Wirel Commun Lett, 2014, 3: 653–656
32 Yoo T, Goldsmith A. On the optimality of multiantenna broadcast scheduling using zero-forcing beamforming. IEEE J Sel Areas Commun, 2006, 24: 528–541